Applied Catalysis B: Environmental 333 (2023) 122787

Contents lists available at ScienceDirect

Applied Catalysis B: Environmental

journal homepage: www.elsevier.com/locate/apcatb

A 3D porous Fe-MoS_2/CMF catalyst for high-efficient catalytic reforming of lignin vapor by microwave irradiation

Wenliang Wang [a,*], Jiale Huang [a], Yishuai Fu [a], Weikun Jiang [b,*], Yutong Chen [a], Yujun Ma [a], Sizhe Han [a]

[a] College of Bioresources Chemical and Materials Engineering (College of Flexible Electronics), Shaanxi University of Science & Technology, Xi'an 710021, China
[b] State Key Laboratory of Biobased Material and Green Papermaking, Key Laboratory of Pulp and Paper Science & Technology of Ministry of Education, Qilu University of Technology (Shandong Academy of Sciences), Ji'nan, Shandong Province 250353, China

ARTICLE INFO

Keywords:
Microwave-assisted depolymerization
Lignin
Catalyst

ABSTRACT

Improving the yield of target monophenols plays an important role in increasing the economic competitiveness of lignin valorization. In this study, a 3D porous Fe-MoS_2/CMF catalyst with nanoflower microstructure was successfully fabricated by a simple one-step hydrothermal method. The catalytic depolymerization of the lignin β-O-4 model showed that Fe-doping increased the efficiency of the catalytic conversion reaction and promoted the cleavage of the β-O-4 ether bond, in agreement with theoretical calculations. Reforming of lignin depolymerization vapor revealed that the Fe-MoS_2/CMF catalysts significantly improved the selectivity of phenol (30.01 wt %) and styrene (16.34 wt%) with the decrease of oligomers. Moreover, finite element simulation showed that the Fe-MoS_2/CMF catalysts can also enhancing the local thermal effect by creating hot spots on the surface, thereby facilitate the lignin vapor reforming. Consequently, this work provides a promising method for the efficient production of phenol and styrene from lignin using bimetallic nanoarray microwave responsive catalyst.

1. Introduction

Lignin is the main component of lignocellulosic biomass and consists of three major phenolic monomers: coniferyl alcohol, sinapyl alcohol and p-coumaryl alcohol [1]. Due to its abundance of methoxylated phenylpropane structures, lignin is considered as a potential feedstock for replacing petroleum in the production of sustainable aromatic chemicals [2]. However, its complex structure results in low reactivity and high steric hindrance, preventing the effective use of lignin in petrochemical substitutes [3,4]. Commonly used strategies for lignin depolymerization include enzymatic, thermal and catalytic, and the different strategies have a significant impact on product yields and monomer composition [5]. Therefore, the development of effective depolymerization methods to increase the selectivity of aromatic monomers is vital to improve the economic competitiveness of sustainable biomass aromatic chemicals to replace traditional petrochemical aromatic chemicals.

Microwave assisted catalytic depolymerization (MACD) of lignin, an effective way to convert lignin to aromatic compounds, has received considerable attention to obtain high selectivity of aromatic compounds [6–8]. Generally, catalyst plays an important role in MACD process, which largely determines the distribution of product monomer. As an excellent catalyst, MoS_2 has been widely used to supply hydrogen in reductive depolymerization reactions [9–11]. The catalytic activity of MoS_2 is considered to be generated by the coordination of unsaturated Mo sites and S vacancies on the edge [12]. Co-doping of metals can reduce the Mo-S bond energy to increase vacancies and improve catalyst reactivity [13,14]. Ji et al. [10] found that MoS_2/AC catalyst with more edge sites has higher catalytic activity for the depolymerization of lignin to alkylphenols. Zhang et al. [15] prepared Co-MoS_2 catalyst by Co doping and found that the acid sites produced by Co doping can promote the C-O bond cleavage. In addition, our previous work has demonstrated that MoS_2 is not only an excellent microwave absorber but also exhibits high selectivity in the conversion of lignin to phenols [16].

Carbonized melamine-formaldehyde (CMF) resin foam is a low cost, light weight, high porosity carbon-based material. Herein, we demonstrate a one-pot hydrothermal strategy to preparation of Fe-MoS_2/CMF on a flexible 3D carbon matrix. Initially, an intrinsically porous carbon skeleton (CMF) was obtained by high temperature carbonization of melamine-formaldehyde (MF) resin foam to allow the passage of lignin

* Corresponding authors.
E-mail addresses: wangwenliang@sust.edu.cn (W. Wang), weikun0709@126.com (W. Jiang).

https://doi.org/10.1016/j.apcatb.2023.122787
Received 2 December 2022; Received in revised form 17 April 2023; Accepted 19 April 2023
Available online 25 April 2023

vapor. Sequential deposition of Fe-MoS_2 nanosheets was realized through the addition of an Anderson-type polyoxometalate ($(NH_4)_3[FeMo_6O_{24}H_6]\cdot 6\ H_2O$, $FeMo_6$ [17]) so that the deposition process could be completed in a single hydrothermal step. Taking advantage of Fe-doped nanosheet-built Fe-MoS_2 array and 3D macroporous carbon network, the obtained self-supported Fe-MoS_2/CMF composite exhibits high C-O bond cleavage activity and good lignin vapor reforming ability. Microwave assisted catalytic depolymerization (MACD) using Fe-MoS_2/CMF catalyst delivers high selectivity for reforming lignin vapor to phenol and styrene.

2. Method and experimental

2.1. Materials

Melamine-formaldehyde (MF) resin sponge was purchased from cleanwrap Co., Ltd (Shanghai, China). $(NH_4)_6Mo_7O_{24}\cdot 4\ H_2O$, $Fe(NO_3)_3\cdot 9\ H_2O$, $FeSO_4\cdot 7\ H_2O$, methanol and thiourea were all purchased from Damao Chemical Reagent Factory (Tianjin, China). $Na_2S_2O_3\cdot 5\ H_2O$ was purchased from Tianli Chemical Reagent Co., Ltd (Tianjin, China). All the reagents were used as received without further purification. DI water was utilized throughout the experiment. Lignin (dealkaline), CAS: 9005–53–2, was purchased from TCI Development Co (Shanghai). Microwave absorbent of SiC (α-SiC) was purchased from the Aladdin Industrial Corporation (Shanghai).

2.2. Catalyst preparation

2.2.1. Preparation of CMF

The preparation of CMF is as follows: The MF was cut into several pieces ($2 \times 2 \times 2\ cm^3$) , washed with DI water and absolute ethanol respectively, and then carbonized in two steps. In the first step, the temperature was raised to 250 ℃ at 1 ℃/min and kept for 60 min; in the second step, the temperature was raised to 700 ℃ at 2 ℃/min and kept for 2 h; after carbonization, the temperature was reduced to room temperature at the rate of 10 ℃/min to obtain CMF. The whole carbonization process was carried out under a nitrogen atmosphere.

2.2.2. Preparation of Fe-MoS_2/CMF

A hydrothermal approach was used to obtain Fe-MoS_2/CMF. First, 40 mL of deionized aqueous solution containing $FeMo_6$ (120.1 mg, 0.1 mmol) and thiourea (91.3 mg, 1.2 mmol) was prepared via vigorous stirring. Then the obtained solution and 3 pieces of CMF ($1 \times 1 \times 1\ cm^3$) were put into a 50 mL Teflon-lined stainless-steel autoclave to react at 180 ℃ for 24 h. After cooling to room temperature, the obtained product was washed with DI water for several times and dried in a vacuum oven at 60 ℃ for 12 h to obtain Fe-MoS_2/CMF. The load mass of Fe-MoS_2/CMF (51.45%) was obtained by weighing the sample mass before and after material deposition.

For comparison, MoS_2/CMF and FeS_2/CMF were obtained by the same preparation method as Fe-MoS_2/CMF (detailed methods were shown in supporting information). The sulfide loading of MoS_2/CMF and FeS_2/CMF were 56.72% and 74.51%, respectively.

2.3. Catalyst characterization

A scanning electron microscope (SEM, Hitachi S4800, Japan) and transmission electron microscope (TEM, FEI Tecnai G2-F20, America) were used to investigate the morphology of the samples. X-ray diffraction (XRD) was used to study the crystal structures of the Catalysts on a Bruker D8 Advance diffractometer (Germany) in the 2θ range of 10–80° at room temperature (Cu Kα radiation, $\lambda = 1.5418$ Å). Xray photoelectron spectroscopy (XPS) was performed on a Shimadzu AXIS $SUPRA^+$ (Japan).

2.4. Catalytic depolymerization reaction

100 mg of lignin β-O-4 model compound and 10 mg catalyst (Fe-MoS_2/CMF, MoS_2/CMF and FeS_2/CMF, respectively) were added to 30 mL methanol. Synthesis methods of all three lignin model compounds were showed in supporting information. The mixed solution was placed in a 50 mL high flux batch reactor system (Parr). After the reactor was sealed, it was purged with nitrogen three times to remove air, and then reacted at 128 bar nitrogen and 260 ℃ for 6 h. After the reaction completed, wait for the reactor to cool to room temperature and separate liquid and solid samples.

The structures of the three lignin models used are shown in Fig. S1a-c, including two model dimers (2-phenoxy-1-phenylethanol, guaiacyl glycerol-β-guaiacyl ether) and a G-type model polymer (GMP).

2.5. Microwave assisted catalytic depolymerization (MACD) method

A microwave reactor with a dynamic vapor flow reaction system was used for MACD experiments. The configuration of the reactor is shown in Fig. 1. 15 g of lignin (dealkaline) was mixed well with 15 g of microwave absorbents (SiC), and this mixture was placed into the glass sleeve of the reactor. The Fe-MoS_2/CMF (200 mg) was placed on the other side of the glass sleeve and separated from the lignin mixture by a glass wall with connecting holes. Nitrogen gas was introduced into the reactor for 30 min to eliminate the air in the reactor. Added methanol (CH_3OH) to the gas-washing bottle and constant the N_2 flow at 600 mL/min. Adjust the microwave power to 1000 W (2.45 GHz) until the temperature reaches 600 ℃, and kept the reaction temperature for 15 min. After the reactor temperature was lower than 100 ℃, the solid product was obtained from the glass sleeve. The volatile vapor was rapidly condensed in circulating ethanol at (-20 ± 1) ℃ to obtain MACD oil. The liquid product obtained without the involvement of the catalyst is called MAD oil. In order to obtain insoluble lignin oligomer, diethyl ether insoluble phase (DEIP) was extracted from the separated 30 wt% liquid product with diethyl ether, and the degraded product was further removed by water for subsequent testing.

2.6. Product analysis

To analyze the liquid products, take 1 mL of the obtained solution and add 0.3 μL n-decane (as internal standard). The solution was analyzed using GC-2014 (Shimadzu, Japan) equipped with HP5 column and flame ionization detector (FID). The temperature of the injection port was set to 280 ℃. The column temperature was set as: hold at 50 ℃ for 5 min, raise the temperature from 50 ℃ to 280 ℃ (5 ℃/min), and then hold for 7 min. Similarly, the same liquid sample as GC-FID was used for GC-MS (Agilent 7890B series, America) analysis. The injection temperature was 280 ℃. The column temperature program was: hold at 50 ℃ for 5 min, then raise the temperature from 50 ℃ to 280 ℃ (5 ℃/min), and 280 ℃ (7 min). Set the ion source temperature at 230 ℃ and the EI source electron energy of 70 eV.

The monomer was determined by comparing the corresponding relationship between GC-MS and GC-FID spectra. The monomer yield was calculated according to the area of monomer and the area of n-decane in GC chromatogram by using the quantitative method of effective carbon number (ECN). Referring to the previous calculation method, the specific calculation method was shown in supporting information [16].

Matrix-assisted laser desorption/ionization-time of flight (MALDI-TOF) mass spectroscopy was used to detect the molecular weight distribution of oligomers in DEIP. MALDI-TOF (Bruker ultraflex) was set as follows: 200 Hz pulsed ND:YAG laser (355 nm) voltage polarity negative, 20 kV acceleration voltage, and the matrix is CHCA (α-Cyano-4-hydroxycinnamic acid).

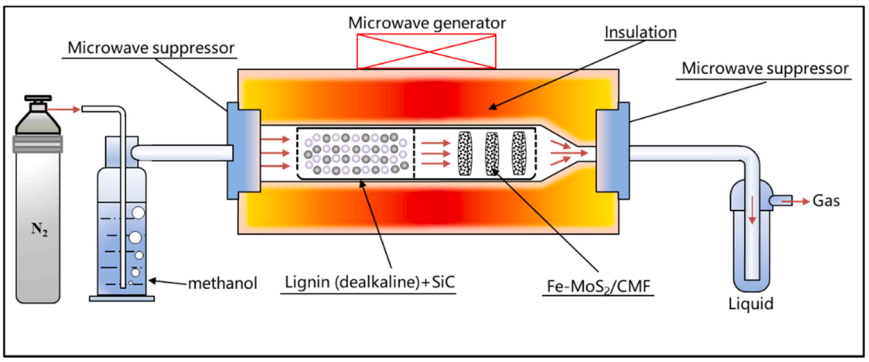

Fig. 1. Schematic diagram of the Fe-MoS_2/CMF catalyst MACD modes.

2.7. *Physicochemical calculation and simulation*

Physicochemical calculation and simulation were carried out by density functional theory (DFT) calculations and Multiphysics numerical modeling. The Vienna ab initio simulation package (VASP) was used to perform DFT calculations to understand the reaction mechanism of Fe-

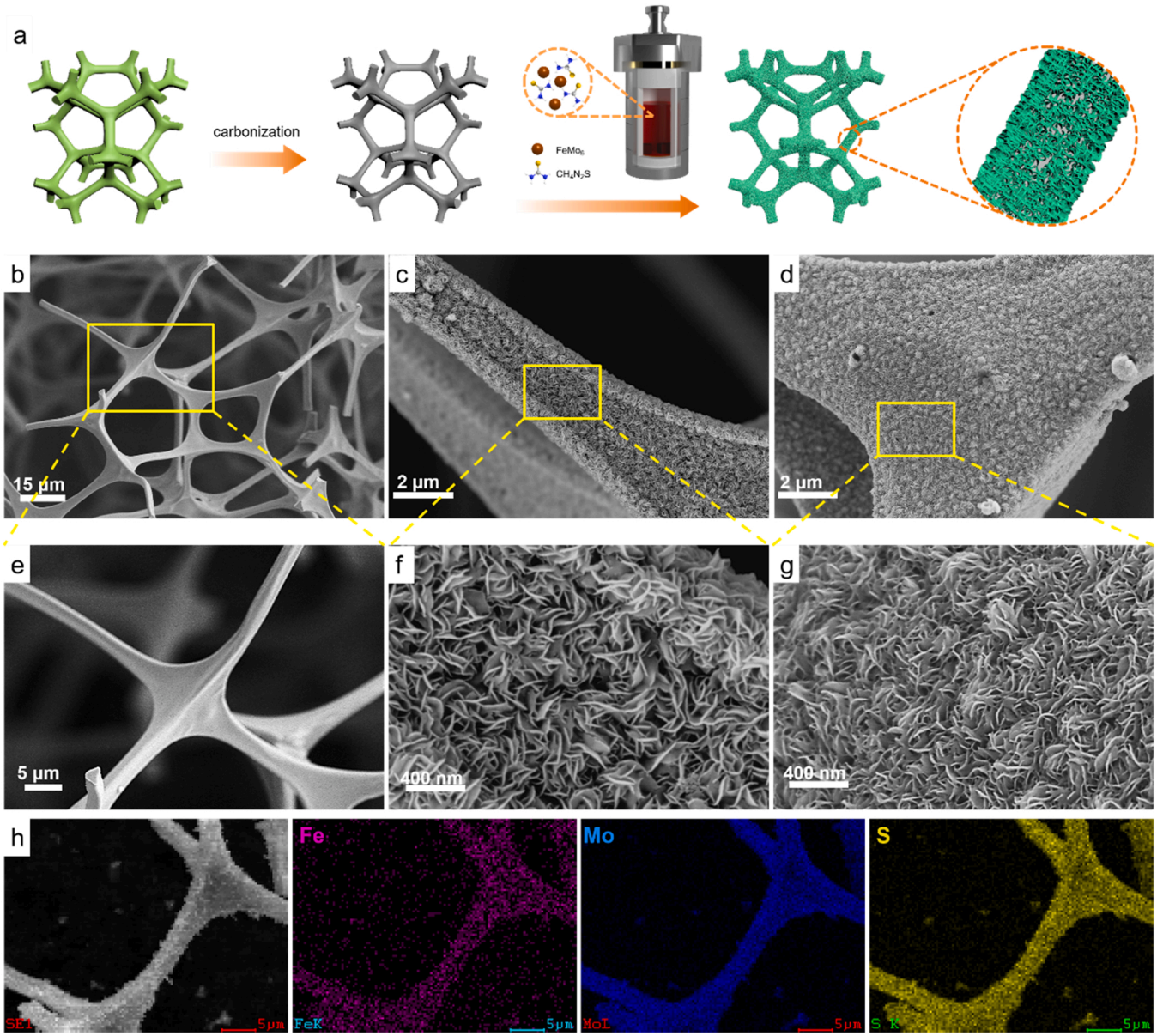

Fig. 2. (a) Synthetic Strategy of Fe-MoS_2/CMF catalyst; (b, e) SEM images of CMF at different magnification; SEM images of Fe-MoS_2/CMF (c, f) and MoS_2/CMF (d, g) at different magnification; (h) SEM image and the corresponding elemental mapping images of Fe, Mo and S for Fe-MoS_2/CMF.

MoS_2/CMF for β-O-4 bond cleavage. Finite element analysis and modeling was performed using COMSOL v.5.6 software. Catalyst model (100 ×100 ×100 μm^3) and nanoflower surface models were established respectively to study microwave-assisted reaction.

3. Results and discussion

3.1. Synthesis and characterization of catalyst

As shown in Fig. 2a, a two-step strategy including carbonization and deposition was introduced to obtain the Fe-MoS_2/CMF catalyst. Firstly, 3D porous MF was carbonized into CMF at 700 ℃, and the volume decreased slightly with the color changing from white to black (Fig. S2a). Afterward, the CMF serving as a skeleton was homogeneously coated with Fe doped MoS_2 after a one-step hydrothermal growth to obtain the Fe-MoS_2/CMF catalyst. The prepared Fe-MoS_2/CMF can be placed on dandelion and has good flexibility, as shown in Fig. S2b-c. After pressing under pressure, Fe-MoS_2/CMF fully recovered to its original shape. The surface morphology of the MF, CMF and Fe-MoS_2/CMF were examined by scanning electron microscopy (SEM). MF (Fig. S3a-b) and CMF (Fig. 2b, and Fig. 2e) show a 3D interconnected network composed with a smooth flat surface, which can provide great support for the loading of nanostructure [18]. The morphology of the catalysts loaded with Fe-MoS_2 nanoflowers are shown in Fig. 2c and Fig. 2f, formed by nanoflowers that can buffer volume changes and attached to the CMF network. The SEM images of MoS_2/CMF are as shown in Fig. 2d and Fig. 2g. Fe-MoS_2 nanoflowers are mainly composed of MoS_2 crystal phase (Fig. 3c), resulting in the morphology of Fe-MoS_2/CMF basically consistent with MoS_2/CMF. The prepared FeS_2/CMF is shown as Fig. S3c-d, where the surface of the CMF is unevenly covered by polyhedral FeS_2. The corresponding element mapping of Mo, Fe and S confirmed the uniform distribution of Fe-MoS_2 nanoflowers on CMF (Fig. 2h).

The TEM images (Fig. 3a) of the Fe-MoS_2/CMF further demonstrated the successful synthesis of Fe-MoS_2 nanoflowers, which consists of nanosheets with a width of ca. 300 nm. The HRTEM images of Fe-MoS_2/CMF (Fig. 3b) showed the lattice distance of 0.62 nm and 0.27 nm, which belong to the (002) lattice plane of MoS_2 and the (200) lattice plane of FeS_2, respectively, demonstrating the successful formation of nanoflowers by MoS_2 and FeS_2 together. To further validate the successful synthesis of the catalyst, the crystallinity and phase purity of the synthesized Fe-MoS_2/CMF, MoS_2/CMF and FeS_2/CMF were investigated through X-ray diffraction (XRD) analysis. As shown in Fig. 3c, both Fe-MoS_2/CMF and MoS_2/CMF show distinct peaks centered at 14.4°, representing the (002) planes of MoS_2 (JCPDS, card NO.65–1951). Moreover, peaks centered at 33.0°, 37.0° and 56.3° on Fe-MoS_2/CMF can be assigned to the (200), (210), and (311) lattice planes of FeS_2 (JCPDS, card NO.65–1211). As a comparison, Fig. S4 shows the XRD pattern of FeS_2/CMF, consisting of pyrite (JCPDS, card no. 65–1211) and marcasite (JCPDS, card no. 37–0475).

The XPS measurement spectrum in Fig. 4a further determines the presence of molybdenum, ferrum and sulfur. The Mo 3d scanning spectrum can be distinguished into six characteristic peaks (Fig. 4b). The two peaks of 228.5 eV and 231.7 eV are characteristic of Mo^{4+} species [19]. The existence of 227.6 eV and 230.8 eV are attributed to Mo^{2+} species. And 235.0 eV originates from Mo^{6+} species and obtained by oxidation of Mo^{4+} exposed to air [20]. The S 2 s peak (225.1 eV) near the Mo 3d region indicates the presence of Mo-S bonds in CMF [21]. The XPS spectrum of S 2p in Fig. 4c is deconvoluted into four peaks, corresponding to S^{2-} $2p_{3/2}$ of 159.0 eV, S^{2-} $2p_{1/2}$ of 160.2 eV, S_2^{2-} $2p_{1/2}$ of 161.2 eV and 166.6 eV of satellite peak respectively. Generally, S_2^{2-} $2p_{1/2}$ is related to sulfur defects, indicating the presence of terminal unsaturated S atoms, and the existence of satellite peak is due to the oxidation of sulfide [22,23]. Fig. 4d shows the XPS spectrum of Fe with three characteristic peaks, in which 708.9 eV, 712.1 eV and 724.3 eV correspond to Fe^{2+} $2p_{3/2}$, Fe^{3+} $2p_{3/2}$ and Fe^{2+} $2p_{1/2}$ species, respectively. The existence of Fe^{2+} characteristic peak and the S_2^{2-} characteristic peak both demonstrate the formation of FeS_2 [24]. These XPS analyses show that both Fe and Mo have excellent binding with S, which demonstrate the successful preparation of Fe-MoS_2/CMF.

3.2. Depolymerization of β-O-4 model compound

As the most abundant substructure, the effective cleavage of the β-O-4 linkage is important for understanding the technical lignin depolymerization. Model compounds research approach offers an effective method for studying relatively simple reactions in complicated lignin system. To clarify the effect of Fe-MoS_2/CMF on β-O-4 linkage cleavage, 2-phenoxy-1-phenylethanol was selected for catalytic depolymerization to investigate the catalytic activities of the catalysts. In order to better reproduce the process of lignin depolymerization, guaiacylglycerol-β-Guaiacyl ether with more side chains was also selected for catalytic depolymerization reaction. Further, GMP was synthesized to examine the effect of Fe-MoS_2/CMF on molecular chain length of lignin. All depolymerization experiments adopt the same conditions.

The depolymerization products and yields of model 2-phenoxy-1-phenylethanol (1a) with different catalysts are shown in Table 1. In a blank experiment without any catalyst (as shown in entry 1), the yield of phenol was 28.08% at a steady pressure (128 bar) and temperature (260 ℃). Obviously, the existence of Mo species increased the

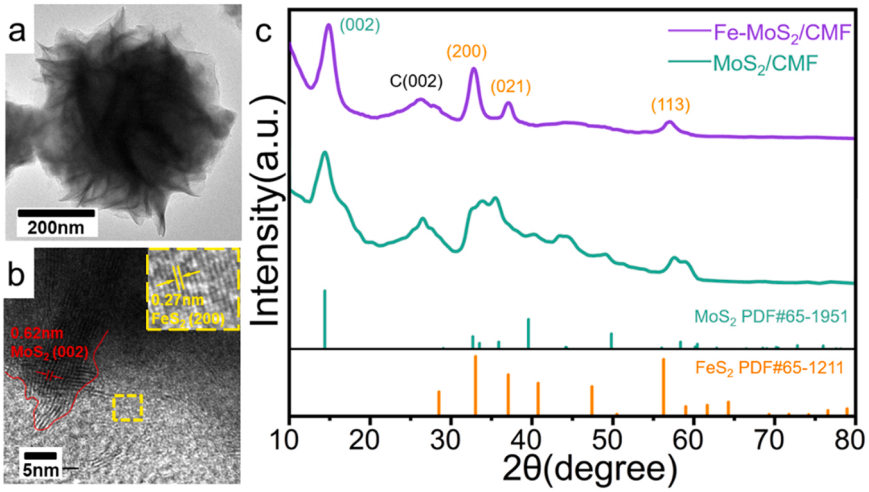

Fig. 3. (a) TEM image of Fe-MoS_2/CMF nanoflower; (b) HRTEM images of Fe-MoS_2/CMF; (c) XRD patterns of Fe-MoS_2/CMF and MoS_2/CMF.

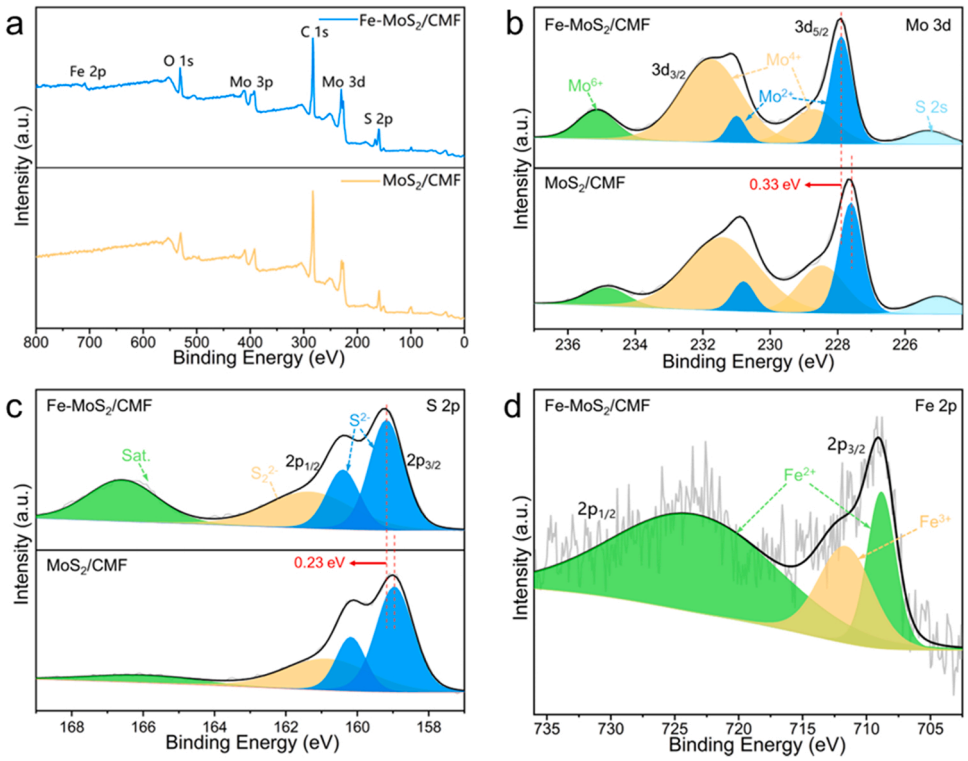

Fig. 4. (a) The XPS survey of Fe-MoS_2/CNF and MoS_2/CNF. The high-resolution spectra of (b) Mo 3d, (c) S 2p for Fe-MoS_2/CNF and MoS_2/CNF, (d) Fe 2p for Fe-MoS_2/CNF.

Table 1
Main products and yields of 2-phenoxy-1-phenylethanol (1a) depolymerized with different catalysts.

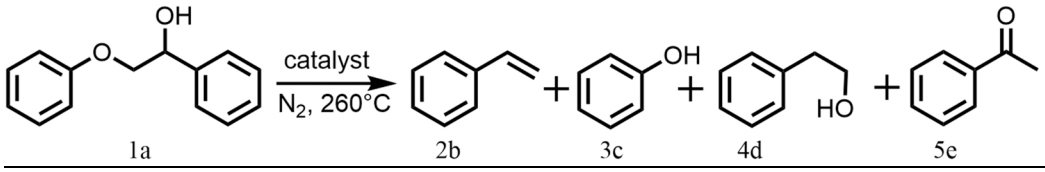

1a 2b 3c 4d 5e

Entry	catalyst	Conv. (%)	Yield (%)				
			2b	3c	4d	5e	others
1	None	83.45	12.05	28.08	10.15	10.39	39.33
2	Fe-MoS_2/CMF	94.12	15.87	36.80	15.70	12.25	19.38
3	MoS_2/CMF	92.51	16.37	35.44	14.62	11.89	21.68
4	FeS_2/CMF	85.54	24.84	27.68	10.84	8.16	28.48

Reaction conditions: 100 mg 2-phenoxy-1-phenylethanol, 10 mg catalyst (deposition mass), 30 mL solvent methanol, 260 ℃, 128 bar N2, 6 h. 1a: 2-Phenoxy-1-phenylethanol; 2b: Styrene; 3c: phenol; 4d: 2-Phenylethanol; 5e: Acetophenone.

conversion rate of 2b to 16.37% (entry 3), indicating that the Mo-S interface plays a positive role in the cleavage of β-O-4 linkage. The doping of Fe enhances the ability of the Mo-S interface to provide hydrogen radicals, so that the Fe-MoS_2/CMF catalyst has the highest yield of principal products (2b-5e) and exhibits the highest selectivity for 3c. In entry 4, FeS_2/CMF significantly improved the selectivity of 2b, which is considered to the removal of C-O by the hydrodeoxygenation of free Fe^{2+} ions in the methanol solution. As expected, $FeMoS_2$/CMF provides the highest conversion of 94.12%, demonstrating that the formation of the Mo-Fe interface enhanced the catalytic performance of the Mo-S catalyst [12].

The depolymerization product yields of guaiacylglycerol-β-guaiacyl ether (6 f) are shown in Table 2. The conversion rate of 6 f is higher than that of 1a because there are more electron withdrawing groups in its benzene ring and C_γ to promote the cleavage of β-O-4 bond. Similarly, due to the promotion of catalytic ability by Mo-Fe interface, Fe-MoS_2/CMF still shows the highest conversion rate of 6 f (98.71%). The low yield of 7 g is due to the polycondensation of guaiacol into dimer during the depolymerization process. Polycondensation is inevitable due to the existence of catalyst acid sites [25]. But the highest yield of 7 g in entry 2 indicates that the hybridization of Fe to Mo-S can reduce the occurrence of the polycondensation reaction. Compared with none catalyst (entry 1), Fe-MoS_2/CMF significantly improves the yield of 8 h (21.34%) without affecting the yield of other main products.

In order to explore the influence of catalyst on the polymerization relationship in lignin, the catalytic performance of Fe-MoS_2/CMF on GMP was investigated. Monomer products and yields of catalytic depolymerization of GMP are shown in Table 3. The increase of polymerization degree obviously increases the depolymerization resistance and reduces the conversion of products. As the β-O-4 bond cleavage products of GMP, the yields of acetovanillone(16.59%) and homovanillyl alcohol (12.15%) have effectively improved under the catalysis

Table 2
Main products and yields of guaiacylglycerol-β-guaiacyl ether (6 f) depolymerized with different catalysts.

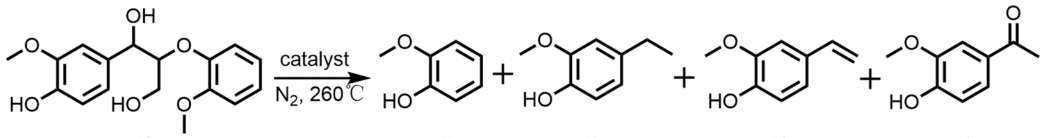

6f 7g 8h 9i 10j

Entry	catalyst	Conv. (%)	Yield (%)				
			7 g	8 h	9i	10j	others
1	None	91.45	14.36	10.77	22.28	20.54	32.05
2	Fe-MoS_2/CMF	98.71	17.14	21.34	24.10	20.29	17.13
3	MoS_2/CMF	97.18	13.43	17.89	21.24	22.87	24.57
4	FeS_2/CMF	92.15	11.11	11.09	32.36	17.73	27.71

Reaction conditions: 100 mg guaiacylglycerol-β-guaiacyl ether, 10 mg catalyst (deposition mass), 30 mL solvent methanol, 260 ℃, 128 bar N2, 6 h. 6 f: Guaiacylglycerol-β-guaiacyl ether; 7 g: Guaiacol; 8 h: 4-Ethyl-2-methoxyphenol; 9i: 4-Hydroxy-3-methoxystyrene; 10j: Acetovanillone.

Table 3
Monomer product and yields of catalytic depolymerization of GMP.

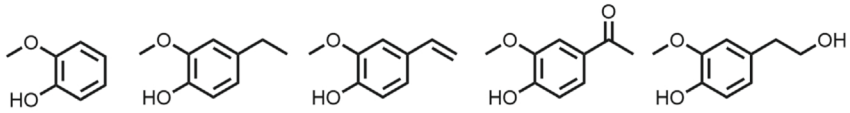

7g 8h 9i 10j 11k

Entry	Catalyst	Conv. (%)	Yield (%)				
			7 g	8 h	9i	10j	11k
1	None	69.72	5.43	9.71	19.36	11.31	13.53
2	Fe-MoS_2/CMF	86.88	6.92	17.12	25.20	12.15	16.59

Reaction conditions: 100 mg GMP, 10 mg catalyst (deposition mass), 30 mL solvent methanol, 260 ℃, 128 bar N2, 6 h.

of Fe-MoS_2/CMF. Obviously, the performance of Fe-MoS_2/CMF for the catalytic cleavage of β-O-4 bonds and the provision of hydrogen radicals are still significant in the conversion of lignin with high degree of polymerization.

3.3. Microwave-assisted catalytic depolymerization of lignin

Based on depolymerization study of model compounds, Fe-MoS_2/CMF catalysts capable of efficiently cleaving the β-O-4 bond appear to be promising catalysts for the reductive depolymerization of lignin. Thus, the performance of Fe-MoS_2/CMF catalysts in the catalytic depolymerization of lignin was investigated. In the experiments, the Fe-MoS_2/CMF catalyst was placed at the back end of the glass sleeve. It has been proved that relatively complete oligomer can be obtained using dimethyl ether to extract DEIP [26,27]. The oligomers were obtained by extracting the liquid products with diethyl ether, and the molecular weight change of lignin oligomer under the action of catalysts were obtained by MALDI-TOF analysis. As a typical lignin subunit, phenylpropane guaiacol has a molecular weight of 166 g/mol [28]. Therefore, signals in the *m/z* range of 250–350 can be attributed to lignin dimer, and the *m/z* range of more than 350 can be attributed to lignin trimers and tetramers or larger polymers. In Fig. 5, the MAD oil consists mainly of trimers, with tetramers also exists in the MAD oil product. Compared with MAD oil, the main products of MACD oil are dimer, and the content of trimer is very low. The small signal of MACD oil indicates that Fe-MoS_2/CMF has a significant decomposition effect on oligomer. The competitive relationship between the interconversion of monophenols and oligomers means that promoting the decomposition reaction of oligomers leads to an increase in the production of monophenols.

The distribution of lignin depolymerization products is shown in Fig. 6a. The catalysis of Fe-MoS_2/CMF on lignin vapor leads to more monomer side chains fragmentation, thus reducing the yield of liquid oil (from 26.97 wt% to 22.58 wt%) and promoting the generation of gas. In addition, the production of small hydrocarbon molecules from side chain fracture also increases the gas yield. The relative content of each component of the liquid products are shown in Fig. 6b, and detailed product yields are shown in Table S1. The addition of Fe-MoS_2/CMF catalyst significantly reduced the relative content of carbonyl compounds and promoted the production of hydrocarbons (HCs). This is attributed to the promotion of deoxidation by the acid sites of the catalyst and the internal porous structure [29,30].

The selectivity of monophenols under the action of Fe-MoS_2/CMF are shown in Fig. 6c. The addition of Fe-MoS_2/CMF drives the formation of

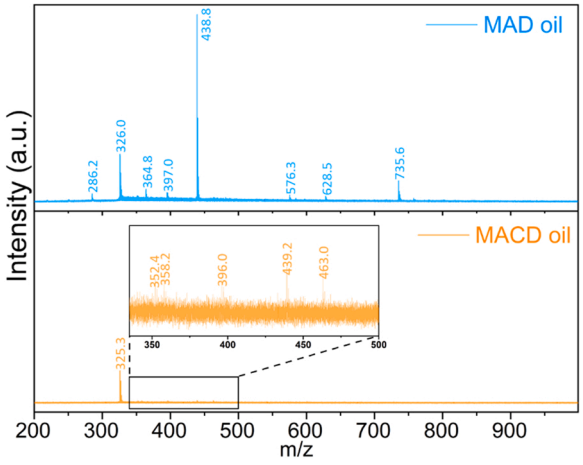

Fig. 5. MALDI-TOF spectra of lignin oligomers extracted from depolymerization liquid oil.
MAD: Microwave assisted depolymerization; MACD: Microwave assisted catalytic depolymerization.

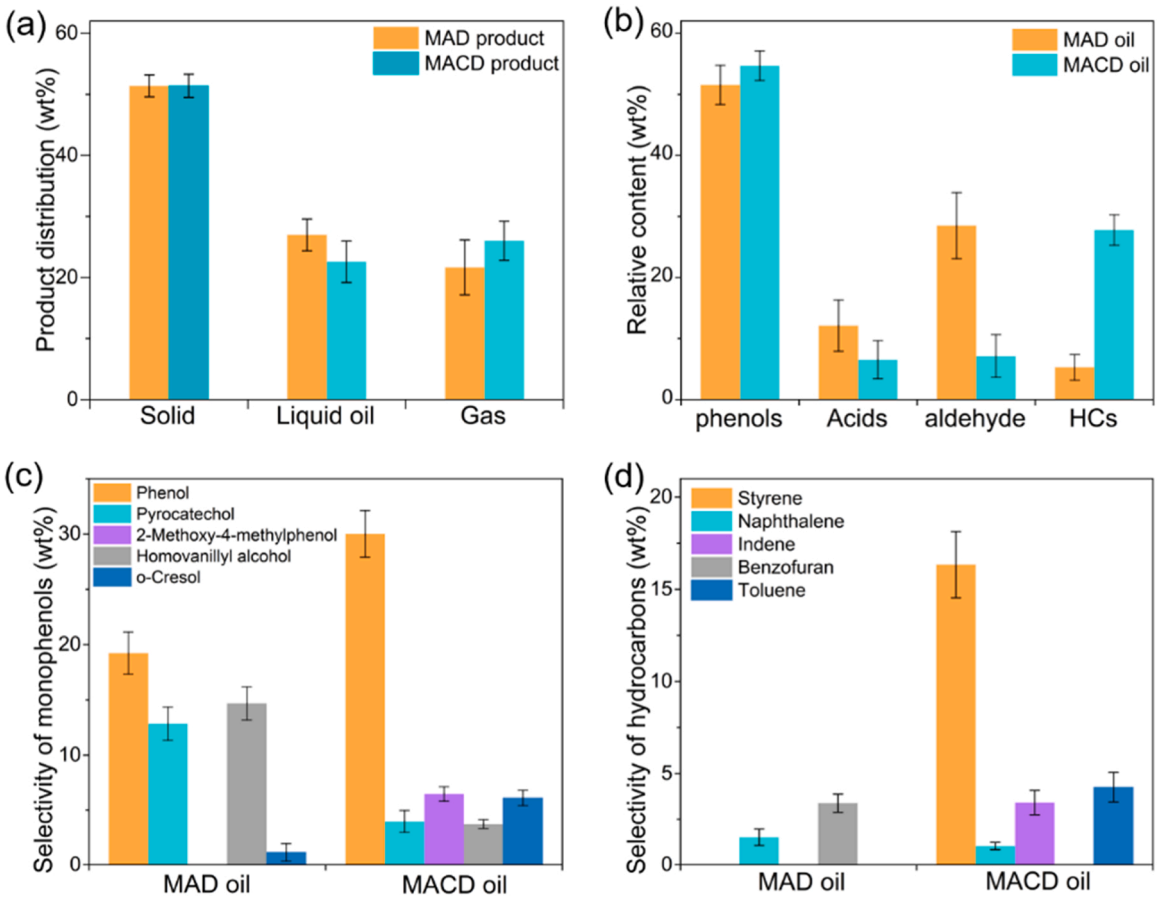

Fig. 6. (a) Product distribution of MAD and MACD reaction; MAD oil and MACD oil for (b) component distribution; (c) phenolic selectivity; (d) hydrocarbon selectivity. Reaction conditions: 15 g lignin (dealkaline), 15 g SiC, 200 mg Fe-MoS_2/CMF, 600 ℃, CH_3OH, 15 min.
MAD: Microwave assisted depolymerization; MACD: Microwave assisted catalytic depolymerization; HCs: Hydrocarbon.

2-methoxy-4-methylphenol and *o*-Cresol due to the deoxygenation and decarbonylation of the branched chains. The selectivity and species of alkylphenols that are significantly reduced in MACD oils equally demonstrate the good hydrogenation ability of Fe-MoS_2/CMF. On the complex surface of Fe-MoS_2/CMF, alkylphenols are adsorbed to the acid center, leading to dehydration, cracking, dealkylation, isomerization, decarboxylation and oligomerization [31]. Interestingly, the selectivity of phenol in MACD oil increased to 30.01% (compared with 19.23% of MAD oil), which improved the economic attractiveness of MACD oil. The possible reason is that the deoxidation active center formed at the Fe-Mo interface to adsorb alkyl phenol for deoxygenation, following hydrogenates methoxy group and promotes the cleavage of alkyl-branched chain [10,32].

The selective of hydrocarbons in liquid products are shown in Fig. 6d. In the absence of the catalyst, small amounts of naphthalene and benzofuran were detected in the MAD oil. And naphthalene also exists in MACD oil, as polycondensation is unavoidable. The study of Ma et al. and Xue et al. on the deoxidation of porous catalysts shows that oxygenated compounds will be deoxidized to phenols on porous catalysts and eventually converted to aromatics [29,31]. This is also confirmed by the increased types and selectivity of hydrocarbons in MACD oil. It is worth noting that the selectivity of styrene in all hydrocarbons is up to a rare 16.34 wt%. This protonation leads to the formation of carbocation within the lignin side chain, which then react further by way of a β-hydrogen elimination reaction to form styrene [33].

3.4. Influence of microwave irradiation on MACD process by physicochemical numerical modeling

It is well known that the decisive step energy barrier is an important factor in limiting the reaction rate. The decomposition reactions of 2-phenoxy-1-phenylethanol with three different catalysts are shown in Fig. 7a. We simulate the adsorption properties of each compound on three catalyst crystal planes in the catalytic depolymerization of 2-phenoxy-1-phenylethanol, and obtained the most stable adsorption configuration (Fig. S5). To compare the catalytic performance of the three catalysts, MoS_2 (002 crystal plane), FeS_2 (200 crystal plane) and Fe-doped MoS_2 (002 crystal plane) were selected and the Gibbs free energy distribution of the reaction was obtained by DFT calculations (Fig. 7b). The energy required for the decisive step (E_{ds}) is Fe-MoS_2 (1.675 eV) < MoS_2 (3.007 eV), which implies that the Fe-MoS_2 crystal faces are more favorable than MoS_2 for the breakage of the β-O-4 ether bond. In contrast, the catalytic activity of FeS_2 was not as high as expected from the calculations, it is considered that the polyhedral crystal structure greatly reduced the catalytic activity of FeS_2 lacking S vacancies.

Although microwaves have been used in many chemical reactions, the interaction between microwave irradiation and chemical substances still needs further exploration [34]. To illustrate the ability of microwave irradiation to initiate or activate multiphase catalysts, we present here a tentative mechanistic model of microwave-initiated for hydrogen production using Fe-MoS_2 catalysts (Fig. 8).

In microwave electromagnetic radiation, Fe-MoS_2 nanoparticles absorb microwaves and convert microwaves into energy due to its high microwave absorption capacity [16]. The difference in electromagnetic

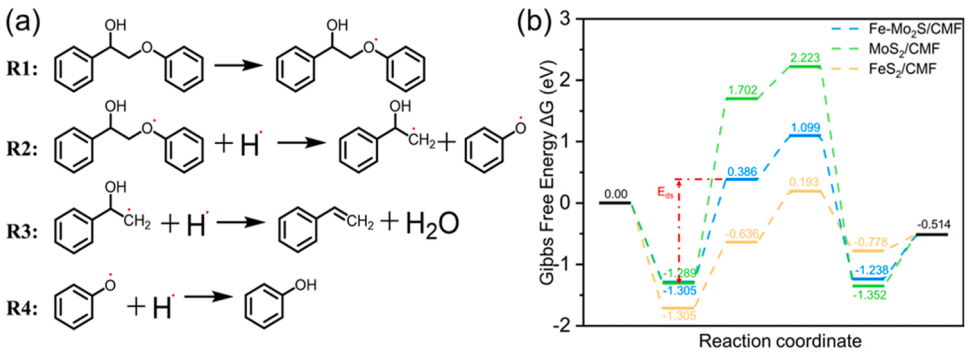

Fig. 7. (a) Decomposition pathway of 2-phenoxy-1-phenylethanol in the presence of three catalyst; (b) Potential energy profile of 2-phenoxy-1-phenylethanol initial decomposition on three different catalysts.

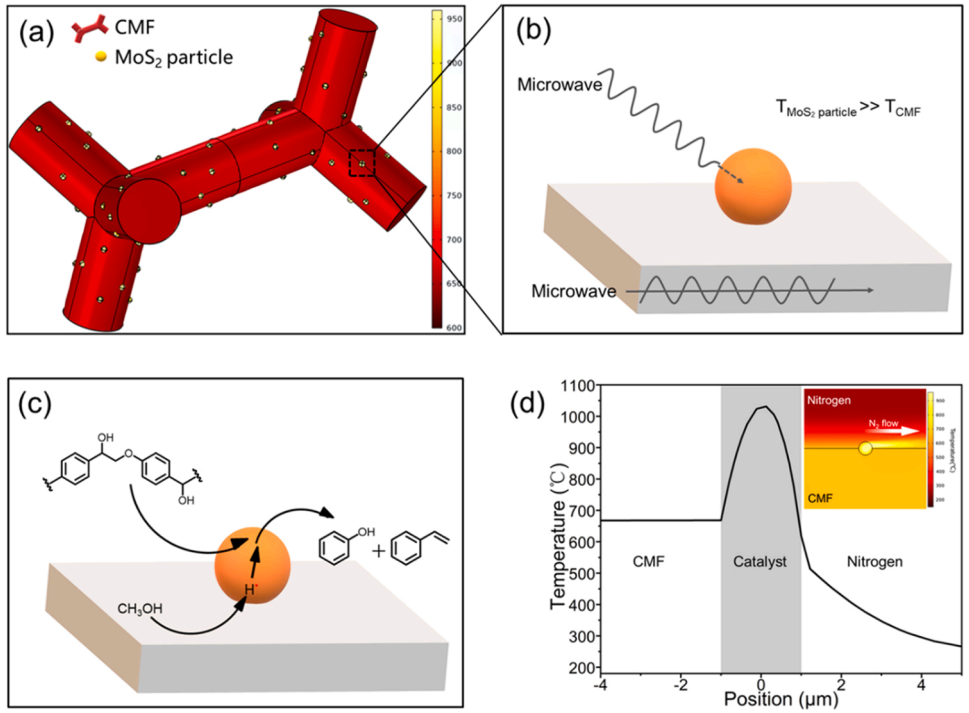

Fig. 8. (a) The finite element simulation model of the catalyst under the set conditions; (b)The temperature gap between the CMF skeleton and nanoparticles under microbial radiation; (c) Microwave initiation for hydrogen and microwave-catalyzed fracture of C-O bonds by Fe-MoS_2 nanoparticles; (d) Modelling of the heating rate at the nanoparticle. MW, microwave.

properties between the carbon matrix and Fe-MoS_2 nanoparticles allows the Fe-MoS_2 nanoparticles to reach a higher temperature than the carbon matrix (Fig. 8a-b). Therefore, Fe-MoS_2 nanoparticles will support the lignin vapor crossing the catalyst surface with sufficiently low activation energy (Fig. 7) to allow high frequency collisions of the vapor with the catalyst active site, which in turn leads to an increase in the pre-finger factor A in the Arrhenius reaction equation ($k = Ae^{-E_a/RT}$). In addition, hydrogen radicals can also decrease the activation barrier and reform the lignin vapors into aryl monomers [35]. Ultimately, the catalyst is able to significantly facilitate the catalytic reaction under the synergistic effect of temperature and microwave electromagnetic radiation (Fig. 8c).

In Fig. 8d, we show a representative finite element simulation model mapping of the heating rate at the interface between Fe-MoS_2 nanoparticles and the carbon matrix. Based on the excellent microwave absorption properties of MoS_2, hot spots are preferentially formed inside the nanoparticles, resulting in high local temperatures. Related computational and experimental studies of microwave-assisted catalysis show that the electric field not only affects the multiphase catalytic activity and selectivity, but also improves the efficiency of reforming for deoxygenation and further promotes the reaction.

4. Conclusions

In summary, we present an effective microwave reforming method for transforming lignin vapor into specific target monophenols and aromatic hydrocarbons by the developed Fe-MoS_2/CMF catalyst. The properties of MoS_2 confer excellent lignin vapor reforming ability to the catalyst, and Fe doping further enhances the catalytic performance of Fe-MoS_2/CMF by lowering the energy barrier. Microwave-assisted catalytic depolymerization of lignin vapor using Fe-MoS_2/CMF was found to exhibit particularly high selectivity of phenol (30.01%) and styrene (16.34%). Overall, this work presents a promising approach for the preparation of specific platform compounds from lignin using microwave-assisted depolymerization of bimetallic catalysts.

CRediT authorship contribution statement

Wenliang Wang: Conceptualization, Supervision, Writing – review & editing, Funding acquisition, Project administration. **Jiale Huang:** Conceptualization, Data curation, Formal analysis, Writing – original draft. **Yishuai Fu:** Visualization, Investigation. **Weikun Jiang:** Synthetic lignin model compounds. **Yutong Chen:** Data curation, Software, Visualization. **Yujun Ma:** Investigation. **Sizhe Han:** Software, Visualization.

Declaration of Competing Interest

The authors declare that they have no known competing financial interests or personal relationships that could have appeared to influence the work reported in this paper.

Data Availability

Data will be made available on request.

Acknowledgements

This work was financially supported by the National Natural Science Foundation of China (31800497) and by the Foundation (No. KF201917) of the Key Laboratory of Pulp and Paper Science and Technology of the Ministry of Education of China.

Appendix A. Supporting information

Supplementary data associated with this article can be found in the online version at doi:10.1016/j.apcatb.2023.122787.

References

[1] M. Ko, L.T.M. Pham, Y.J. Sa, J. Woo, T.V.T. Nguyen, J.H. Kim, D. Oh, P. Sharma, J. Ryu, T.J. Shin, S.H. Joo, Y.H. Kim, J.W. Jang, Unassisted solar lignin valorisation using a compartmented photo-electro-biochemical cell, Nat. Commun. 10 (2019) 5123.
[2] C.C. Almada, A. Kazachenko, P. Fongarland, D.D. Perez, B.N. Kuznetsov, L. Djakovitch, Supported-metal catalysts in upgrading lignin to aromatics by oxidative depolymerization, Catalyst 11 (2021) 467.
[3] W. Schutyser, T. Renders, S. Van den Bosch, S.F. Koelewijn, G.T. Beckham, B. F. Sels, Chemicals from lignin: an interplay of lignocellulose fractionation, depolymerisation, and upgrading, Chem. Soc. Rev. 47 (2018) 852–908.
[4] Y. Zhang, J.C. Mao, W.K. Jiang, S. Zhang, L. Tong, J.H. Mao, G. Wei, M. Zuo, Y. H. Ni, Lignin sulfonate induced ultrafast polymerization of double network hydrogels with anti-freezing, high strength and conductivity and their sensing applications at extremely cold conditions, Compos. Part B Eng. 217 (2021), 108879.
[5] D. Bourbiaux, J.J. Pu, F. Rataboul, L. Djakovitch, C. Geantet, D. Laurenti, Reductive or oxidative catalytic lignin depolymerization: an overview of recent advances, Catal. Today 373 (2021) 24–37.
[6] L. Shuai, M.T. Amiri, Y.M. Questell-Santiago, F. Heroguel, Y.D. Li, H. Kim, R. Meilan, C. Chapple, J. Ralph, J.S. Luterbacher, Formaldehyde stabilization facilitates lignin monomer production during biomass depolymerization, Science 354 (2016) 329–333.
[7] X.D. Liu, F.P. Bouxin, J.J. Fan, R. Gammons, V.L. Budarin, C.W. Hu, J.H. Clark, Effect of metal triflates on the microwave-assisted catalytic hydrogenolysis of birch wood lignin to monophenolic compounds, Ind. Crops Prod. 167 (2021), 113515.
[8] P. Dhar, R. Vinu, Microwave-assisted catalytic solvolysis of lignin to phenols: kinetics and product characterization, ACS Omega 3 (2018) 15076–15085.
[9] A.H. Zacher, M.V. Olarte, D.M. Santosa, D.C. Elliott, S.B. Jones, A review and perspective of recent bio-oil hydrotreating research, Green Chem. 16 (2014) 491–515.
[10] N. Ji, X.Y. Diao, X.X. Li, Z.C. Jia, Y.J. Zhao, X.B. Lu, C.F. Song, Q.L. Liu, C.Z. Li, Toward alkylphenols production: lignin depolymerization coupling with methoxy removal over supported MoS_2 catalyst, Ind. Eng. Chem. Res. 59 (2020) 17287–17299.
[11] N.X. Li, L.F. Wei, R. Bibi, L.Y. Chen, J.H. Liu, L. Zhang, Y.Q. Zheng, J.C. Zhou, Catalytic hydrogenation of alkali lignin into bio-oil using flower-like hierarchical MoS_2-based composite catalysts, Fuel 185 (2016) 532–540.
[12] X.Y. Diao, N. Ji, X.X. Li, Y. Rong, Y.J. Zhao, X.B. Lu, C.F. Song, C.X. Liu, G.Y. Chen, L.L. Ma, S.R. Wang, Q.L. Liu, C.Z. Li, Fabricating high temperature stable Mo-Co_9S_8/Al_2O_3 catalyst for selective hydrodeoxygenation of lignin to arenes, Appl. Catal. B Environ. 305 (2022), 121067.
[13] Y.C. Huang, Y.H. Sun, X.L. Zheng, T. Aoki, B. Pattengale, J.E. Huang, X. He, W. Bian, S. Younan, N. Williams, J. Hu, J.X. Ge, N. Pu, X.X. Yan, X.Q. Pan, L. J. Zhang, Y.G. Wei, J. Gu, Atomically engineering activation sites onto metallic 1T-MoS_2 catalysts for enhanced electrochemical hydrogen evolution, Nat. Commun. 10 (2019) 982.
[14] W.J. Song, S.J. Zhou, S.H. Hu, W.K. Lai, Y.X. Lian, J.Q. Wang, W.M. Yang, M. Y. Wang, P. Wang, X.M. Jiang, Surface engineering of CoMoS nanosulfide for hydrodeoxygenation of lignin-derived phenols to arenes, ACS Catal. 9 (2019) 259–268.
[15] Y.J. Zhang, T.K. Liu, Q.N. Xia, H.Y. Jia, X.L. Hong, G.L. Liu, Tailoring of surface acidic sites in Co-MoS_2 catalysts for hydrodeoxygenation reaction, J. Phys. Chem. Lett. 12 (2021) 5668–5674.
[16] W.L. Wang, Z.H. Ma, X.J. Zhao, S.W. Liu, L.P. Cai, S.Q. Shi, Y.H. Ni, Effect of various microwave absorbents on the microwave-assisted lignin depolymerization process, ACS Sustain. Chem. Eng. 8 (2020) 16086–16090.
[17] T.T. Kenji Nomiya, Takahiro Shirai, Makoto Miwa, Anderson-type heteropolyanions of molybdenum(VI) and tungsten(VI), Polyhedron 6 (1987) 213–218.
[18] J. Yan, Y. Huang, C. Chen, X.D. Liu, H. Liu, The 3D CoNi alloy particles embedded in N-doped porous carbon foams for high-performance microwave absorbers, Carbon 152 (2019) 545–555.
[19] J. Jia, W.J. Zhou, Z.Q. Wei, T.L. Xiong, G.X. Li, L.L. Zhao, X.F. Zhang, H. Liu, J. Zhou, S.W. Chen, Molybdenum carbide on hierarchical porous carbon synthesized from Cu-MoO_2 as efficient electrocatalysts for electrochemical hydrogen generation, Nano Energy 41 (2017) 749–757.
[20] F.X. Xi, P. Bogdanoff, K. Harbauer, P. Plate, C. Holm, J. Rappich, B. Wang, X. Y. Han, R. van de Krol, S. Fiechter, Structural transformation identification of sputtered amorphous MoS_X as an efficient hydrogen-evolving catalyst during electrochemical activation, ACS Catal. 9 (2019) 2368–2380.
[21] L.Q. Wu, X.B. Xu, Y.Q. Zhao, K.Y. Zhang, Y. Sun, T.T. Wang, Y.Q. Wang, W. Zhong, Y.W. Du, Mn doped MoS_2/reduced graphene oxide hybrid for enhanced hydrogen evolution, Appl. Surf. Sci. 425 (2017) 470–477.
[22] Y. Li, K. Yin, L.L. Wang, X.L. Lu, Y.Q. Zhang, Y.T. Liu, D.F. Yan, Y.Z. Song, S.L. Luo, Engineering MoS_2 nanomesh with holes and lattice defects for highly active hydrogen evolution reaction, Appl. Catal. B Environ. 239 (2018) 537–544.
[23] J.H. Lin, P.C. Wang, H.H. Wang, C. Li, X.Q. Si, J.L. Qi, J. Cao, Z.X. Zhong, W.D. Fei, J.C. Feng, Defect-rich heterogeneous MoS_2/NiS_2 nanosheets electrocatalysts for efficient overall water splitting, Adv. Sci. 6 (2019) 1900246.
[24] J. Sun, C.W. Liu, W.H. Kong, J. Liu, L.Y. Ma, S. Li, Y.H. Xu, Rational design of FeS_2 microspheres as high-performance catalyst for electrooxidation of hydrazine, J. Mater. Sci. Technol. 110 (2022) 161–166.
[25] X.J. Yang, M.Q. Feng, J.S. Choi, H.M. Meyer, B. Yang, Depolymerization of corn stover lignin with bulk molybdenum carbide catalysts, Fuel 244 (2019) 528–535.
[26] X.H. Zhang, H. Ma, S.B. Wu, Effects of temperature and atmosphere on the formation of oligomers during the pyrolysis of lignin, Fuel 268 (2020), 117328.
[27] X.H. Zhang, H. Ma, T.F. Li, S.B. Wu, Oligomers obtained from sequential fractionation of lignin pyrolysis oil, Energy Convers. Manag. 201 (2019), 112181.
[28] A. Toledano, L. Serrano, A. Pineda, A.A. Romero, R. Luque, J. Labidi, Microwave-assisted depolymerisation of organosolv lignin via mild hydrogen-free hydrogenolysis: catalyst screening, Appl. Catal. B Environ. 145 (2014) 43–55.
[29] S. Xue, Z.Y. Luo, Q.G. Zhou, H.R. Sun, L.W. Du, Regulation mechanism of three key parameters on catalytic characterization of molybdenum modified bimetallic micro-mesoporous catalysts during catalytic fast pyrolysis of enzymatic hydrolysis lignin, Bioresour. Technol. 337 (2021), 125396.
[30] X.F. Xue, C.S. Zhang, D. Xia, Y.G. Wang, J. Liang, Y.F. Sun, Dual-catalyst catalytic pyrolysis of poplar sawdust: A systematic study on first-layered catalysts, Chem. Eng. J. 431 (2022), 134251.
[31] Z.Q. Ma, E. Troussard, J.A. van Bokhoven, Controlling the selectivity to chemicals from lignin via catalytic fast pyrolysis, Appl. Catal. A Gen. 423 (2012) 130–136.
[32] Z.X. Yang, A. Kumar, A. Apblett, Integration of biomass catalytic pyrolysis and methane aromatization over Mo/HZSM-5 catalysts, J. Anal. Appl. Pyrolysis 120 (2016) 484–492.
[33] D.J. Mihalcik, C.A. Mullen, A.A. Boateng, Screening acidic zeolites for catalytic fast pyrolysis of biomass and its components, J. Anal. Appl. Pyrolysis 92 (2011) 224–232.
[34] X.Y. Jie, W.S. Li, D. Slocombe, Y.G. Gao, I. Banerjee, S. Gonzalez-Cortes, B.Z. Yao, H. AlMegren, S. Alshihri, J. Dilworth, J. Thomas, T.C. Xiao, P. Edwards, Microwave-initiated catalytic deconstruction of plastic waste into hydrogen and high-value carbons, Nat. Catal. 3 (2020) 902–912.
[35] W.L. Wang, X.B. Wang, Z.H. Ma, C. Duan, S.W. Liu, H.L. Yu, X.P. Li, L.P. Cai, S. Q. Shi, Y.H. Ni, Breaking the lignin conversion bottleneck for multiple products: co-production of aryl monomers and carbon nanospheres using one-step catalyst-free depolymerization, Fuel 285 (2021) 119211–119218.